Alkali Metal Cation Interactions with 12-Crown-4 in the Gas Phase: Revisited

P. B. Armentrout,[a] C. A. Austin,[b] and M. T. Rodgers[b]

[a] *Department of Chemistry, University of Utah, Salt Lake City, UT 84112.*

[b] *Department of Chemistry, Wayne State University, Detroit, Michigan 48202*

***Abstract*:** Quantitative interactions of alkali metal cations with the cyclic 12-crown-4 polyether ligand (12C4) are studied. Experimentally, Rb^+(12C4) and Cs^+(12C4) complexes are formed using electrospray ionization and their bond dissociation energies (BDEs) determined using threshold collision-induced dissociation of these complexes with xenon in a guided ion beam tandem mass spectrometer. The energy-dependent cross sections thus obtained are interpreted using an analysis that includes consideration of unimolecular decay rates, internal energy of the reactant ions, and multiple ion-neutral collisions. 0 K BDEs of 151.5 ± 9.7 and 137.0 ± 8.7 kJ/mol, respectively, are determined and exceed those previously measured by 60 and 54 kJ/mol, respectively, consistent with the hypothesis proposed there that excited conformers had been studied. In order to provide comparable thermochemical results for the Na^+(12C4) and K^+(12C4) systems, the published data for these systems are reinterpreted using the same analysis techniques, which have advanced since the original data were acquired. Revised BDEs for these systems are obtained as 243.9 ± 12.6 and 182.0 ± 17.3 kJ/mol, respectively, which are within experimental uncertainty of the previously reported values. In addition, quantum chemical calculations are conducted at the B3LYP and MP2(full) levels of theory with geometries and zero point energies calculated at the B3LYP level using both HW*/6-311+G(2d,2p) and def2-TZVPPD basis sets. The theoretical results are in reasonable agreement with experiment, with B3LYP/def2-TZVPPD values being in particularly good agreement. Computations also allow the potential energy surfaces for dissociation of the M^+(12C4) complexes to be elucidated. These are used to help explain why the previous studies formed excited conformers of Rb^+(12C4) and Cs^+(12C4) but apparently not of Na^+(12C4) and K^+(12C4).

Keywords: 12-crown-4, alkali metal cations, crown ethers, guided ion beam, thermochemistry

Introduction

In molecular recognition [1-5], crown ethers are a prototypical "host" accommodating many different "guest" species, of which the alkali metal cations are exemplary. First characterized by Pedersen in 1967 [6,7], crown ethers have found widespread applications, for example as carriers to facilitate amino acid and drug transfer across membranes [8], to transport therapeutic radiation to tumor sites [9], to design novel materials for isotope separation [10-12], in the development of advanced analytical methods [13], and as phase transfer catalysts to facilitate dissolution of metals in nonpolar solvents [14].

In order to quantitatively understand the host-guest interactions that underlie all of these applications, it is useful to have gas-phase data that allow the effects of the intrinsic mutual affinities to be separated from effects of solvation of the separated species and their complexes. To this effect, More, Ray, and Armentrout systematically determined the bond dissociation energies (BDEs) for the gas-phase interactions of all five alkali metal cations with the crown ethers, 12-crown-4 (12C4 = 1,4,7,10-tetraoxacyclododecane), 15-crown-5 (15C5 = 1,4,7,10,13-pentaoxacyclopenta-decane), and 18-crown-6 (18C6 = 1,4,7,10,13,16-hexaoxacyclooctadecane), and compared these results with those for multiple smaller but related ligands, dimethyl ether (DME) and dimethoxyethane (DXE or diglyme) [15-20]. This effort was aided by parallel computational studies of Feller and coworkers [15,16,21]. Their general finding was that the BDEs of all of these ligands decreased as the size of the metal ion increased, consistent with binding energies that are dominated by electrostatic effects. Furthermore, it could be shown that the sum of BDEs for four DME ligands versus two DXE ligands versus 12C4 decreased, indicating that the backbones of the latter two ligands impose constraints on the orientations of the oxygen atoms. Thus, the free ligands can bind at both optimal bond distances from the metal cation and orient their local dipole moments to optimize the binding, whereas the multidentate ligands cannot. Although the individual gas-phase M^+–crown BDEs show no selectivity for particular sized cations, by combining these quantitative data with similar hydration energies of the alkali metal cations, it was shown that the selectivity (for instance, for K^+ by 18C6) arises

UU IR Author Manuscript

from the competition between complexation by the crown versus hydration [22]. Thus, by breaking down the aqueous thermochemistry into its components, the details of the driving forces for these host-guest interactions could be understood more completely.

In these early studies, it was found that the experimental BDEs for all ligands bound to Li^+, Na^+, and K^+ agreed well with theoretical calculations [15-18], as did values for DME ligands to Rb^+ and Cs^+ [19]. Notably, experimental BDEs for the multidentate DXE and 12C4 ligands with Rb^+ and Cs^+ were much lower than theoretical values [19,21]. A number of explanations for these differences were explored and it was concluded that excited conformers of these complexes were being generated, such that the experimental dissociation energies did not correspond to the global ground state on the potential energy surface. This hypothesis was plausible as these complexes were formed in a dc discharge flow-tube (DC-FT) ion source in which the metal cations and ligands were condensed with one another in a gas-phase environment and then thermalized by collisions with the He/Ar flow gases. In such a source, it is possible for complexes in excited conformations to get collisionally trapped and dominate the observed collision-induced dissociation (CID) behavior because the energy required for their decomposition is lower than for the ground-state conformation.

In the present paper, the complexes of Rb^+ and Cs^+ with 12C4 are generated using an electrospray ionization (ESI) source in which the preformed complexes are extracted from solution, such that the ground-state species are expected to be formed. As in the earlier experiments, these complexes are then subjected to CID with Xe as a function of kinetic energy and the resultant cross sections analyzed to extract the metal cation – 12C4 binding energies. In addition to these new data for Rb^+ and Cs^+, the original data for the M^+(12C4) where $M^+ = Na^+$, K^+, Rb^+, and Cs^+ complexes are reanalyzed using more advanced analysis tools that have been developed in the interim, in order to ensure that the present thermochemical information for the various alkali metal cations is self-consistent. (The original crown ether studies were among the earliest that used the phase space limit approach described further below.) Finally, higher level calculations of the BDEs as well as the complete potential energy surfaces for all four metal

UU IR Author Manuscript

cations interacting with 12C4 are conducted for comparison to the experimental results. Good agreement is now found for all four complexes, verifying that the present bond energies are accurate and correspond to the ground-state conformers in all cases.

Experimental and Computational Section

General Experimental Procedures. Cross sections for CID of the rubidium and cesium cation complexes with 12C4 are measured using the Wayne State University guided ion beam tandem mass spectrometer that has been described in detail previously [23]. Experiments are conducted using an electrospray ionization (ESI) source under conditions similar to those described previously [24]. Briefly, the ESI is operated using a 50:50 by volume H_2O/MeOH solution with ~5×10^{-4} M 12C4 and 5×10^{-4} M RbCl or CsCl (all chemicals were purchased from Sigma-Aldrich). All other operating conditions are similar to those used previously. Notably the ESI/ion funnel/radio frequency (rf) hexapole source arrangement used here has been shown to produce ions thermalized to 300 K [24-29]. Additional details of the source can be found in the Supplementary Data.

M^+(12C4) complexes are extracted from the source, focused, accelerated, and mass selected using a magnetic momentum analyzer. The mass-selected ions are decelerated to a well-defined kinetic energy and focused into a rf octopole ion guide that traps the ions radially. The octopole passes through a static gas cell containing xenon, which is used as the collision gas because it is heavy and polarizable, leading to more efficient kinetic to internal energy transfer [30,31]. After collision, the reactant and product ions drift to the end of the octopole where they are extracted and focused into a quadrupole mass filter for mass analysis. The ions are detected with a high voltage dynode, scintillation ion detector [32] and the signal is processed using standard pulse counting techniques. Ion intensities, measured as a function of collision energy, are converted to absolute cross sections as described previously [33]. The uncertainty in relative cross sections is approximately ±5% and that for the absolute cross sections is approximately ±20%. The ion kinetic energy distribution is measured to be Gaussian and has a typical fwhm of

UU IR Author Manuscript

0.3 – 0.5 eV (lab). Uncertainties in the absolute energy scale are approximately ±0.05 eV (lab). Ion kinetic energies in the laboratory frame are converted to energies in the center-of-mass (CM) frame using $E_{CM} = E_{lab}\, m/(m+M)$, where M and m are the masses of the ionic and neutral reactants, respectively. All energies herein are reported in the CM frame unless otherwise noted.

Thermochemical Analysis. Threshold regions of the CID reaction cross sections are modeled using procedures developed elsewhere [34-38], as described previously for similar systems [39-50]. Details of the analysis procedure, which includes explicitly accounting for internal and translational energy distributions [51], the effects of multiple collisions [52], and the lifetime of the dissociating ions, can be found in the Supplementary Data. Notably the utilization of a phase space limit (PSL) approach for analyzing the CID cross sections for heterolytic bond dissociations [53], such as those discussed here, have advanced since the early applications described in the previous M^+-12C4 work. To ensure that the present results for Rb^+ and Cs^+ are self-consistent with the previous work, the previous data for Na^+ and K^+ are reanalyzed using the same methods.

Computational Details. All theoretical calculations were performed using the Gaussian09 suite of programs [54]. Several levels of theory were applied. Initial calculations were performed using density functional theory (DFT) at the B3LYP/HW*/6-311+G(2d,2p) level [55-57]. This level of theory has been shown to provide reasonably accurate structural descriptions of comparable metal-ligand systems [26,42,43,45,58-61]. HW* indicates that Rb and Cs were described using the effective core potentials (ECPs) and valence basis sets of Hay and Wadt [62] (equivalent to the LANL2DZ basis set) with single d polarization functions (exponents of 0.24 and 0.19, respectively) added [63]. Relative energies are determined using single point energies determined at the B3LYP and MP2(full) levels using the HW*/6-311+G(2p,2d) basis set. For calculations on complexes of Na^+ and K^+, the all electron 6-311+G(2d,2p) basis sets were used for comparable calculations. Zero-point vibrational energy (ZPE) corrections were determined using vibrational frequencies calculated at the B3LYP/HW*/6-311+G(2d,2p) level scaled by a factor of 0.98 [64]. Previous work on the

UU IR Author Manuscript

interactions of Rb^+ and Cs^+ with amino acids have demonstrated that the absolute BDEs determined using the Hay-Wadt ECP/valence basis sets do not agree with experiment particularly well [48,50]. Therefore calculations were repeated for each complex as well as those for Na^+ and K^+ using the def2-TZVPPD basis set for all atoms [65]. A mixed basis set with def2-TZVPPD on the metal and 6-311+G(2d,2p) on all other elements was also used for some calculations. Def2-TZVPPD is a balanced basis set on all atoms at the triple-zeta level including two polarization and diffuse functions and uses ECPs on rubidium and cesium developed by Leininger et al. [66]. The def2-TZVPPD basis set was obtained from the EMSL basis set exchange library [67,68]. Geometry optimizations and vibrational frequencies were calculated at the B3LYP/def2-TZVPPD, with zero point energies being scaled by 0.98, and single point energies were also calculated using MP2(full) with the B3LYP geometries. Perhaps not surprisingly, the results using the def2-TZVPPD and mixed def2/6-311+G(2d,2P) basis sets provide very similar results (deviations < 2 kJ/mol for BDE values and < 1 kJ/mol for counterpoise corrected BDEs) and hence only those for the slightly larger def2-TZVPPD basis set are reported below.

For all calculated BDEs, basis set superposition errors (BSSEs) were estimated using the full counterpoise method [69,70], which will be indicated by (cp). For the MP2 single-point energies, the BSSE corrections range from 14 – 25 kJ/mol, whereas for the B3LYP single-point energies, BSSE corrections vary between 1 – 3 kJ/mol for all structures examined here. It has been previously suggested that the full counterpoise approximation to BSSE can provide worse agreement with experiment than MP2 theoretical values without BSSE corrections [71-74]. Because of this tendency for BSSE to overcorrect for the MP2 calculations, the "best" MP2 values may fall between the MP2 values with and without the BSSE corrections, and therefore both values are reported here.

Results

Theoretical Results for 12C4. Several conformations of the free 12-crown-4 ligand are

shown in Figure 1, as calculated at the B3LYP/6-311+G(2d,2p) level of theory. The ground-state structure has S_4 symmetry with alternate oxygens pointing to opposite sides of the ring, which minimizes the dipole-dipole interactions, such that it has no permanent dipole moment. This agrees with previous theoretical results at several levels of theory [21,75,76]. The isotropic polarizability of this species is 17.2 $Å^3$, as calculated at the PBE1PBE/def2-TZVPPD level of theory, a density functional that has been shown to yield polarizabilities that are in good agreement with measured values [77].

Three higher energy structures were also located, with excitation energies ranging from 4 – 46 kJ/mol, Table 1. The lowest of these retains the alternating orientations of the oxygen atoms and has D_{2d} symmetry. It is higher in energy because the lone pair electrons on the opposing oxygen atoms now point towards one another, as opposed to being directed about 45° away from one another in the ground state. There are also structures in which three and four oxygens point to the same side of the ring, thereby increasing the dipole-dipole interactions. These structures have C_s and C_{2v} symmetry, respectively, and lie 9 – 46 kJ/mol higher than the ground-state S_4 conformer.

Theoretical Results for M^+(12C4). Structures of complexes of the four alkali metal cations with 12C4 experimentally studied here were calculated as described above. In the ground-state complex for all metals, the alkali metal cation binds to all four oxygen atoms in a complex having C_4 symmetry, in agreement with the findings of Hill et al. using the RHF/6-31+G(d) level of theory [21]. This tetradentate structure, which we denote C4(++++), is shown for the case of Cs^+ in Figure 2. The nomenclature used here is similar to that devised for our recent study of Zn^{2+} and Cd^{2+} complexes with the crowns but has been simplified somewhat [78]. C4 indicates a four-coordinate complex and the symbols in parentheses indicate the signs of the four ∠OCCO dihedral angles. As will be seen in the following, this is sufficient to uniquely identify the various conformations of the M^+(12C4) complexes located. It should also be noted that there are enantiomers in many cases, e.g., C4(- - - -), which is the mirror image of C4(++++) and therefore has an identical energy. Such enantiomers will not be discussed further.

UU IR Author Manuscript

This figure also provides key geometric information from the B3LYP/def2-TZVPPD calculations for all four metal cations. The four metal-oxygen bond lengths are equal for a given metal and increase as the metal cation gets larger, leading to a decreasing $\angle OM^+O$ bond angle. The increases in the bond lengths closely match the increase in the metal cation radii: 0.98, 1.33, 1.49, and 1.69 Å for Na^+, K^+, Rb^+, and Cs^+, respectively [79]. The geometry of the crown ligand remains largely constant, as shown by the similar CO and CC bond distances and ∠COCC and ∠OCCO dihedral angles. The bond distances are slightly longer than those of the free 12C4 ligand, r_{CO} = 1.420 and 1.422 Å and r_{CC} = 1.516 Å, consistent with some electron transfer from the ligand to the metal cation. As described further below, a key geometric parameter is the angle between the metal cation and the local dipole moment of the oxygen atoms, $\angle M\mu_O$, where 0° indicates alignment. For the C4(++++) complexes, these angles gradually decrease from 47° for the sodium cation complex to 35° for the cesium complex. A comparison with the geometries obtained by Hill et al. at the RHF/6-31+G(d) level of theory [21] can be found in Table S2 of the supplementary data, but the present results generally have slightly shorter MO bond lengths leading to slightly larger $\angle OM^+O$ bond angles. The ∠COCC and ∠OCCO dihedral angles obtained here are also slightly smaller (by 1 – 2°). It seems possible that the geometries of these complexes are not particularly sensitive to the level of theory (including a need for electron correlation) because they are non-covalent interactions between stable singlet species.

We also located two other four-coordinate (C4) structures for all metal complexes, which are distinguished by the OCCO dihedral angles. (The relative energies for all conformers calculated at the B3LYP/def2-TZVPPD level are included in Table S1 with geometric parameters in Table S2 of the Supplementary Data.) C4(+++–) is slightly higher in energy, 8 – 9 kJ/mol, and the C4(+–+–) complex has alternating positive and negative dihedrals leading to C_{2v} symmetry and lies 12 – 18 kJ/mol above the ground state, Table S1. For these two complexes, the M–O bond distances are both shorter and longer and $\angle M\mu_O$ angles are similar to those for the ground state, although longer bonds tend to have smaller $\angle M\mu_O$ angles. Thus, the difference

UU IR Author Manuscript

in energy between the C4 conformers cannot be attributed to the metal-oxygen interactions. Rather the destabilization of the latter species can be attributed to interactions between CH bonds on the carbons adjacent to each oxygen atom. For the C4(++++) ground state, the smallest ∠HCCH dihedral at any oxygen is ~30° for all M^+, whereas these are eclipsed, ∠HCCH = 0°, at all oxygens for the C4(+–+–) conformer. C4(+++–) is an intermediate case possessing both types of dihedrals.

Additional stable conformations were also located for 12C4 complexes with each of the four metal cations, including structures with three (C3), two (C2), or one (C1) strong metal-oxygen interactions. Examples of these structures for the case of Cs^+(12C4) are shown in Figure 3. There are two types of C3 complexes, C3(+++–) and C3(+–+–), where the latter have C_s symmetry (or are very close to C_s symmetry). These are relatively low in energy, lying ~20 and ~32 kJ/mol above the ground state, respectively, with excitation energies largely insensitive to the metal cation, Table S1. Uniquely for the K^+(12C4) complex, the C3(+–+–) intermediate is found to have an imaginary frequency (28 cm^{-1}) corresponding to a ring distortion, but optimizations at lower symmetry do not remove the imaginary frequency. For the C3 complexes, there are three short M–O bond distances associated with $\angle M\mu_O$ angles between 28° and 52°, and one long M–O bond where the $\angle M\mu_O$ angle is now between 74° – 108°, such that the metal is now perpendicular to the dipole moment of these oxygens, Table S2. This perpendicular orientation greatly diminishes the strength of the metal-oxygen interaction.

At higher energies, 42 – 49 kJ/mol above the ground state, the C2 complexes again have C_{2v} symmetry, +–+– ∠OCCO dihedrals, and were also located by Hill et al. [21], where again the bond lengths are slightly longer than the present results, Table S2. Variants of C2 having different dihedrals are not anticipated but a search for such conformations was not conducted. Notably, the "long" M–O bond lengths in these complexes are actually shorter than some of those in the analogous C4 complexes, but the $\angle M\mu_O$ angles associated with these complexes are near 80° instead of the 39 – 48° angles found for the strongly binding oxygens. For Cs^+, we also located a complex containing only one short Cs–O bond length (2.954 Å with the three others

UU IR Author Manuscript

exceeding 4.8 Å), Figure 3. For the smaller metal cations, these C1 species could not be fully converged and collapsed to the C2 complexes during optimization. The relative energies given in Table S1 are for structures that came closest to converging, but in all cases, had an imaginary frequency (52, 18, and 7 cm^{-1} for Na^+, K^+, and Rb^+, respectively), where the motion leads to the C2 complexes.

Theoretical Results for Interconversion of M^+(12C4) Conformations. In addition to these stable species, we also characterized the transition states (characterized by a single imaginary frequency) connecting each of these as well as the product asymptote for all four metal cations. An example of the complete potential energy surface for the case of Cs^+(12C4) is shown in Figure 3. The nomenclature used to identify these transition states (TSs) puts the key geometric parameter that is changing in parentheses, hence, TSC(4–3) indicates that an oxygen is moving from a bonding to a nonbonding position and (+++(+–)) indicates exchange of a positive for a negative OCCO dihedral angle. Transition state barriers between the three C4 conformers range from 29 – 40 kJ/mol, Table S1, increasing slightly as the metal gets larger. There is a transition state that connects C4(++++) and C3(+++–), TSC(4–3)(+++(+–)), and one between C4(+–+–) and C3(+–+–), TSC(4–3)(+–+–), which lie ~30 and 41 – 45 kJ/mol above the ground state, respectively. TSC3(+(+–)+–) connecting C3(+++–) and C3(+–+–) lies somewhat higher, ~54 kJ/mol above the ground state, slightly higher than the energy for converting C3(+-+-) to C2, ~50 kJ/mol. Overall, it can be seen that there are well-defined TSs between the various C4 and C3 conformers and between the C3 and C2 conformers, whereas even in the case of Cs^+(12C4), the TS for conversion of the C2 and C1 conformers lies *below* the energy of C1 once zero point energies are included, Figure 3. Hence the C1 conformer is not actually stable for any of the four metal cations.

Cross Sections for Collision-Induced Dissociation of Rb^+(12C4) and Cs^+(12C4). Kinetic energy-dependent experimental cross sections were obtained for the interaction of Xe with M^+(12C4) where $M^+ = Rb^+$ and Cs^+, as shown in Figure 4. Data shown are results obtained at ~0.2 mTorr of the Xe reactant. The pressure dependence of these cross sections is very small

UU IR Author Manuscript

in both cases. For both complexes, the only dissociation pathway observed was the loss of the intact ligand in the collision-induced dissociation (CID) reactions (1).

$$M^+(12C4) + Xe \rightarrow M^+ + 12C4 + Xe \quad (1)$$

Also shown in Figure 4 are previously published results for both systems. These comparisons clearly show the higher thresholds for the present data. The lower cross section magnitudes observed here are also a direct result of the different energetics as a higher threshold is expected to yield less efficient dissociation.

The models of Eq. (S1) (excluding lifetime effects) and Eq. (S2) (including lifetime effects) were used to analyze zero pressure extrapolated cross sections for reaction (1) for both $M^+(12C4)$ systems. Figure 5 shows that both experimental cross sections are reproduced by Eq. (S2) over a large range of energies (>4 eV) and magnitudes (>2 orders of magnitude). The optimized fitting parameters of Eqs. (S1) and (S2) are provided in Table 2 and were obtained utilizing molecular parameters taken from the B3LYP/def2-TZVPPD calculations. The values of $\Delta S^{\ddagger}_{1000}$, the entropy of activation at 1000 K, which gives some idea of the looseness of the transition states, are also listed in Table 2 and are in the range determined by Lifshitz [80] for simple bond cleavage dissociations. This is reasonable considering that the TSs are assumed to lie at the centrifugal barrier for the association of M^+ + 12C4.

Reanalysis of the Cross Sections for Collision-Induced Dissociation of $M^+(12C4)$. At the time the previous data for the $M^+(12C4)$ complexes were obtained, Rodgers, Ervin, and Armentrout had just developed the statistical approach to analyzing CID cross sections [36]. Hence, these complexes were among the earliest for which our phase space limit (PSL) approach was utilized, sufficiently so that four assumptions regarding the treatment of the transition state (TS) for dissociation were utilized in these early studies: PSL, two "loose" TSs, and a "tight" TS. In the loose TS model, three transitional frequencies in the $M^+(12C4)$ complex were chosen, with one assigned to the reaction coordinate and two (usually hindered rotations) divided by factors of 2 and 10 to give a range in the looseness of the TS, with the average threshold providing E_0(loose). In the tight TS model, only the reaction coordinate frequency is removed in

UU IR Author Manuscript

describing the TS and all other M^+(12C4) reactant frequencies are unchanged, leading to thresholds that are lower limits to the true value. In addition, a fifth assumption (PSLR) was also utilized in analyzing the data for Rb^+(12C4) and Cs^+(12C4), in which the two lowest vibrational frequencies were replaced with the two-dimensional rotational constant of the ligand. This leads to a relatively tight TS and consequently lower threshold energy. In these two cases, the "best" value for the BDE was reported as the average of the PSLR, PSL, and loose TS treatments of the data.

As the implementation of our PSL approach has been refined in subsequent years, we reanalyze the older data here to ensure that comparison between the old and new experimental results and between the experimental results and new theoretical results are self-consistent. Table 3 compares the present analysis with that reported previously for all four metal cation complexes. The data were analyzed using molecular parameters reported in the previous publications as well as those calculated here using B3LYP/def2-TZVPPD. The different sets of molecular parameters make only minor differences in the final results, with the old frequencies yielding lower thresholds by 0.01 eV for Na^+(12C4), 0.05 eV for K^+(12C4), 0.01 eV for Rb^+(12C4), and 0.01 eV for Cs^+(12C4). In the case of Na^+(12C4), the present analysis using the def2 frequencies yields E_0(PSL) = 2.53 ± 0.13 eV. The model of the data, shown in Figure 6a, can be seen to reproduce the data well, actually over a larger energy region than the previous model, although both models are very similar in the critical threshold region. The threshold obtained here is between the previous PSL threshold of 2.61 ± 0.13 eV and E_0(loose) = 2.37 ± 0.21 eV, but within experimental uncertainty of both. The tight threshold of 1.97 ± 0.16 eV is well below these values, as expected for this lower limit to the true threshold value. For K^+(12C4), the present model again reproduces the data over a larger range of energies with a very similar shape to the original model in the threshold region (not shown in Figure 6b). The E_0(PSL) = 1.82 ± 0.10 eV obtained here again falls in between the previously reported E_0(PSL) = 1.96 ± 0.12 eV and E_0(loose) = 1.67 ± 0.16 eV and lies within the combined experimental uncertainties. Notably, neither of these models reproduces a small tail in the data visible only

when expanded by a factor of 10. This tail can be reproduced nicely by shifting the threshold energy down by 0.5 eV, retaining the same value of *n*, and reducing the scaling factor by a factor of ~25 (4%). The model for the tail can then be subtracted from the data and the remaining cross section reanalyzed to yield an alternative interpretation of these data, also listed in Table 3. This approach yields a threshold, 1.96 ± 0.12 eV, reproducing the previous E_0(PSL) value. The sum of these models is shown in Figure 6b and can be seen to reproduce the data throughout the available energy range. We take the average of the analyses in which the tail is ignored and explicitly modeled as our best threshold value including an uncertainty that spans both interpretations, 1.89 ± 0.18 eV.

For the Rb^+(12C4) and Cs^+(12C4) complexes, reanalysis of the old data yields thresholds that lie close to the loose TS results previously reported, Table 3, slightly below the previously reported PSL values, and above the PSLR values, 0.86 ± 0.07 and 0.80 ± 0.05 eV, respectively. In both cases, the present PSL results are within 0.1 eV of the previous "best" values, 0.96 ± 0.13 and 0.88 ± 0.09 eV, respectively, taken as the average of the loose, PSL, and PSLR thresholds.

Conversion from 0 to 298 K. Conversion from 0 K bond energies to 298 K bond enthalpies and free energies is accomplished using the rigid rotor/harmonic oscillator approximation with rotational constants and vibrational frequencies calculated at the B3LYP/def2-TZVPPD level. The resulting ΔH_{298} and ΔG_{298} values along with the conversion factors and 0 K enthalpies measured here for ground-state conformers of all four M^+(12C4) complexes are reported in Table 4. The uncertainties listed are determined by scaling most of the vibrational frequencies by ±10% along with two-fold variations in the metal-ligand frequencies.

Discussion

Comparison of Theoretical and Experimental Bond Dissociation Energies. The theoretical BDEs for the M^+(12C4) complexes, where $M^+ = Na^+$, K^+, Rb^+, and Cs^+, calculated at several levels of theory are compared to the new experimental values in Table 5. The latter include those from the new data for the rubidium and cesium systems, Table 2, and the reanalysis

of the old data for sodium and potassium, Table 3. For the sodium and potassium complexes, B3LYP(cp)/6-311+G(2d,2p) calculations yield 0 K BDEs in reasonable agreement with experiment, lying 11 and 1 kJ/mol *higher* in energy, whereas the B3LYP(cp)/HW*/6-311+G(2d,2p) calculations for rubidium and cesium complexes yield BDE values for M^+(12C4) that are 7 and 17 kJ/mol, respectively, *lower* than experiment. MP2(full)/HW*/6-311+G(2d,2p) results perform reasonably if counterpoise corrected, with potassium showing the largest deviation of 12 kJ/mol. Our MP2 results can be compared favorably to those of Hill, Glendening, and Feller, calculated at the MP2/6-31+G(d)//RHF/6-31+G(d) level [21], Table 5. B3LYP(cp)/def2-TZVPPD results provide BDEs in good agreement with experiment, with the largest deviation being 12 kJ/mol for sodium, within the experimental uncertainty. MP2(full,cp)/def2-TZVPPD results are systematically high, with a 22 kJ/mol deviation for cesium. Overall, mean absolute deviations (MADs) between experiment and theory are excellent for the B3LYP/def2-TZVPPD level of theory whether counterpoise corrected or not, Table 5, with a similarly good MAD obtained for the MP2(full,cp)/HW*/6-311+G(2d,2p) results. MADs for B3LYP/HW*/6-311+G(2d,2p), MP2(full,cp)/def2-TZVPPD, and the results of Hill et al. are about twice as large. Failure to include cp corrections changes the MAD by only 1 kJ/mol for the B3LYP calculations, but the MADs increase to 23 – 38 kJ/mol for the MP2(full) values excluding cp corrections. The comparison between the new experimental BDEs and the def2-TZVPPD results is also shown in Figure 7, where it can be seen that the agreement is excellent, especially for the B3LYP results.

As discussed in the introduction, the low BDEs found previously for Rb^+(12C4) and Cs^+(12C4) were hypothesized to be a result of excited conformations. Here, we also suggest that the small tail in the K^+(12C4) cross section can be identified similarly as a small population of an excited conformer. We can test these suggestions by a comparison of the previous and current BDEs along with the theoretical calculations. As discussed above, a reanalysis of the previous data for CID of Rb^+(12C4) and Cs^+(12C4) yields 0 K thresholds of 0.95 ± 0.07 and 0.87 ± 0.08 eV, respectively, which lie 0.62 ± 0.12 and 0.56 ± 0.12 eV below the values obtained from the

UU IR Author Manuscript

present investigation. Likewise, the tail in the K^+(12C4) data has threshold approximately 0.5 eV below the dominant feature in the cross section. (Notably, identification of the tail in the K^+(12C4) cross section as a small population of an excited conformation shows that there is a gradual change in the behavior of the different metal cations, rather than a sharp differentiation between the smaller and larger metals.) Equating these differences with excitation energies suggests the presence of C2 bidentate conformers, which have calculated energies relative to the C4(++++) tetradentate ground state of 0.48 – 0.51 eV for $M^+ = K^+ – Cs^+$, Table S1. This is consistent with the potential energy surfaces shown in Figure 3 as the C2 complex would be the first formed upon interaction of M^+ with the ground-state conformer of gas-phase 12C4.

These potential energy surfaces are qualitatively consistent with the hypothesis made in the previous work to explain why such excited conformers were observed in the Rb^+(12C4) and Cs^+(12C4) systems. However, there it was also conjectured that the barriers between the higher energy conformers and the ground-state conformer of the complexes varied appreciably with the metal identity as a consequence of the different charge densities. Thus, a lower barrier for the smaller metal cations was conjectured, thereby allowing the initially formed C2 complexes to readily rearrange to the C4 ground states. Table S1 shows that there are not appreciable distinctions in the energies of TSC(3-2) among the different metal cations, and barriers between lower energy conformers are also similar from metal to metal. An alternative explanation for the different behavior of the smaller and larger alkali metal cations relies on the kinetics for stabilization of the M^+(12C4) complexes made by three-body association of M^+ + 12C4 in the flow tube ion source previously used. Because the M^+–12C4 bond energies decrease dramatically for larger cations, the internal energies of the C2 complexes initially formed vary considerably as M^+ changes. Thus, stabilization of the C2 complexes requires fewer collisions with the bath gases present for the larger cations. Furthermore, the weaker binding of the larger alkali metal cations means that there are lower metal-ligand frequencies, increasing the density of states of the C2 complexes, which would decrease the rate of dissociation leading to a longer

UU IR Author Manuscript

lifetime. The longer lifetime means that three-body collisional stabilization of the excited conformation could occur before rearrangement to lower energy conformations.

Conclusions

The present reexamination of the alkali metal cation complexes with the polyether 12-crown-4 have shown that the structures formed are sensitive to the mode of ion formation, as also demonstrated in other systems [26,81-84]. Electrospray ionization clearly forms ground state conformations with no evidence (to better than 1 part in 1000) for the excited conformers formed in a flow-tube source by aggregation of Rb^+ and Cs^+ with 12C4 [19]. An examination of the potential energy surfaces suggests this is not a result of distinctive barriers between the conformers but rather is related to the kinetics of the association process. Reexamination of the previous data for Na^+(12C4) [17] and K^+(12C4) [18] demonstrates that the excited conformer was also present in minor abundance for the potassium complex. Further, we show that the data analysis methods used are robust. Overall, the present experiments for Rb^+(12C4) and Cs^+(12C4) along with a reanalysis of the data for Na^+(12C4) and K^+(12C4) provide reliable thermochemistry for these complexes, as demonstrated convincingly by comparison with high level quantum calculations, Figure 7.

Acknowledgments

This work is supported by the National Science Foundation, CHE-0911191 (MTR) and CHE-1049580 (PBA). A grant of computer time from the Center for High Performance Computing at the University of Utah is gratefully acknowledged. We also thank WSU C&IT for computer time.

Appendix A. Supplementary Data.

Text describing the general experimental procedures and thermochemical analysis procedures used. Tables giving energies and geometries of the various M^+(12C4) species and

the transition states connecting them. Supplementary data associated with this article can be found, in the online version, at doi: xxx.

References

[1] A.D. Buckingham, S.M. Roberts, "Principles of Molecular Recognition", Blackie Academic and Professional, Glassgow, 1993.
[2] R.M. Izatt, J.H. Rytting, D.P. Nelson, B.L. Haymore, J.J. Christensen, Science 164 (1969) 443.
[3] R.M. Izatt, J.S. Bradshaw, S.A. Nielsen, J.D. Lamb, J.J. Christensen, D. Sen, Chem. Rev. 85 (1985) 271.
[4] J.S. Brodbelt, Int. J. Mass Spectrom. 200 (2000) 57.
[5] C.A. Schalley, Int. J. Mass Spectrom. 194 (2000) 11.
[6] C.J. Pedersen, J. Am. Chem. Soc. 89 (1967) 2495.
[7] C.J. Pedersen, Angew. Chem., Int. Ed. Engl. 27 (1988) 1021.
[8] J.-M. Lehn, Angew. Chem., Int. Ed. Engl. 27 (1988) 89.
[9] R.W. Kozak, T.A. Waldmann, R.W. Atcher, O.A. Gansow, Trends Biotechnol. 4 (1985) 259.
[10] E.P. Horwitz, M.L. Dietz, D.E. Fisher, Solvent Extraction and Ion Exchange 9 (1991) 1.
[11] R. Chiarizia, E.P. Horwitz, M.L. Dietz, Solvent Extraction and Ion Exchange 10 (1992) 337.
[12] B.A. Moyer, L.H. Delmau, G.N. Case, S. Bajo, C.F. Baes, Sep. Sci. Technol. 30 (1995) 1047.
[13] J.W. Grate, R. Strebin, J. Janata, O. Egorov, J. Ruzicka, Anal. Chem. 68 (1996) 333.
[14] L.F. Lindoy, The Chemistry Macrocyclic Ligand Complexes, University Press, University Press, Cambridge, UK, 1989.
[15] M.B. More, E.D. Glendening, D. Ray, D. Feller, P.B. Armentrout, J. Phys. Chem. 100 (1996) 1605.
[16] D. Ray, D. Feller, M.B. More, E.D. Glendening, P.B. Armentrout, J. Phys. Chem. 100 (1996) 16116.
[17] M.B. More, D. Ray, P.B. Armentrout, J. Phys. Chem. A 101 (1997) 831.
[18] M.B. More, D. Ray, P.B. Armentrout, J. Phys. Chem. A 101 (1997) 4254.
[19] M.B. More, D. Ray, P.B. Armentrout, J. Phys. Chem. A 101 (1997) 7007.
[20] M.B. More, D. Ray, P.B. Armentrout, J. Am. Chem. Soc. 121 (1999) 417.
[21] S.E. Hill, D. Feller, E.D. Glendening, J. Phys. Chem. A 102 (1998) 3813.
[22] P.B. Armentrout, Int. J. Mass Spectrom. 193 (1999) 227.
[23] M.T. Rodgers, J. Phys. Chem. A 105 (2001) 2374.
[24] R.M. Moision, P.B. Armentrout, J. Am. Soc. Mass Spectrom. 18 (2007) 1124.
[25] S.J. Ye, P.B. Armentrout, J. Phys. Chem. A 112 (2008) 3587.
[26] A.L. Heaton, R.M. Moision, P.B. Armentrout, J. Phys. Chem. A 112 (2008) 3319.
[27] D.R. Carl, R.M. Moision, P.B. Armentrout, Int. J. Mass Spectrom. 265 (2007) 308.
[28] Y. Chen, M.T. Rodgers, J. Am. Chem. Soc. 134 (2012) 2313.
[29] Y. Chen, M.T. Rodgers, J. Am. Chem. Soc. 134 (2012) 5863.
[30] N. Aristov, P.B. Armentrout, J. Phys. Chem. 90 (1986) 5135.
[31] N.F. Dalleska, K. Honma, L.S. Sunderlin, P.B. Armentrout, J. Am. Chem. Soc. 116 (1994) 3519.

[32] N.R. Daly, Rev. Sci. Instrum. 31 (1960) 264.
[33] K.M. Ervin, P.B. Armentrout, J. Chem. Phys. 83 (1985) 166.
[34] S.K. Loh, D.A. Hales, L. Lian, P.B. Armentrout, J. Chem. Phys. 90 (1989) 5466.
[35] F.A. Khan, D.E. Clemmer, R.H. Schultz, P.B. Armentrout, J. Phys. Chem. 97 (1993) 7978.
[36] M.T. Rodgers, K.M. Ervin, P.B. Armentrout, J. Chem. Phys. 106 (1997) 4499.
[37] M.T. Rodgers, P.B. Armentrout, J. Chem. Phys. 109 (1998) 1787.
[38] P.B. Armentrout, K.M. Ervin, M.T. Rodgers, J. Phys. Chem. A 112 (2008) 10071.
[39] F. Meyer, F.A. Khan, P.B. Armentrout, J. Am. Chem. Soc. 117 (1995) 9740.
[40] M.T. Rodgers, P.B. Armentrout, J. Phys. Chem. A 101 (1997) 1238.
[41] H. Koizumi, P.B. Armentrout, J. Am. Soc. Mass Spectrom. 12 (2001) 480.
[42] R.M. Moision, P.B. Armentrout, J. Phys. Chem. A 106 (2002) 10350.
[43] R.M. Moision, P.B. Armentrout, Phys. Chem. Chem. Phys. 6 (2004) 2588.
[44] S.J. Ye, R.M. Moision, P.B. Armentrout, Int. J. Mass Spectrom. 253 (2006) 288.
[45] R.M. Moision, P.B. Armentrout, J. Phys. Chem. A 110 (2006) 3933.
[46] M.T. Rodgers, P.B. Armentrout, Int. J. Mass Spectrom. 267 (2007) 167.
[47] S.J. Ye, A.A. Clark, P.B. Armentrout, J. Phys. Chem. B 112 (2008) 10291.
[48] V.N. Bowman, A.L. Heaton, P.B. Armentrout, J. Phys. Chem. B 114 (2010) 4107.
[49] P.B. Armentrout, E.I. Armentrout, A.A. Clark, T.E. Cooper, E.M.S. Stennett, D.R. Carl, J. Phys. Chem. B 114 (2010) 3927.
[50] P.B. Armentrout, Y. Chen, M.T. Rodgers, J. Phys. Chem. A 116 (2012) 3989.
[51] F. Muntean, P.B. Armentrout, J. Chem. Phys. 115 (2001) 1213.
[52] D.A. Hales, L. Lian, P.B. Armentrout, Int. J. Mass Spectrom. Ion Processes 102 (1990) 269.
[53] P.B. Armentrout, J. Simons, J. Am. Chem. Soc. 114 (1992) 8627.
[54] M.J. Frisch, G.W. Trucks, H.B. Schlegel, G.E. Scuseria, M.A. Robb, J.R. Cheeseman, G. Scalmani, V. Barone, B. Mennucci, G.A. Petersson, H. Nakatsuji, M. Caricato, X. Li, H.P. Hratchian, A.F. Izmaylov, J. Bloino, G. Zheng, J.L. Sonnenberg, M. Hada, M. Ehara, K. Toyota, R. Fukuda, J. Hasegawa, M. Ishida, T. Nakajima, Y. Honda, O. Kitao, H. Nakai, T. Vreven, J. Montgomery, J. A. , J.E. Peralta, F. Ogliaro, M. Bearpark, J.J. Heyd, E. Brothers, K.N. Kudin, V.N. Staroverov, R. Kobayashi, J. Normand, K. Raghavachari, A. Rendell, J.C. Burant, J.M. Millam, S.S. Iyengar, J. Tomasi, M. Cossi, N. Rega, J.M. Millam, M. Klene, J.E. Knox, J.B. Cross, V. Bakken, C. Adamo, J. Jaramillo, R. Gomperts, R.E. Stratmann, O. Yazyev, A.J. Austin, R. Cammi, C. Pomelli, J.W. Ochterski, R.L. Martin, K. Morokuma, V.G. Zakrzewski, G.A. Voth, P. Salvador, J.J. Dannenberg, S. Dapprich, A.D. Daniels, O. Farkas, J.B. Foresman, J.V. Ortiz, J. Cioslowski, D.J. Fox, Gaussian 09, Revision A.02. Gaussian Inc., Pittsburgh, PA, 2009.
[55] A.D. Becke, J. Chem. Phys. 98 (1993) 5648.
[56] C. Lee, W. Yang, R.G. Parr, Phys. Rev. B 37 (1988) 785.
[57] A.D. McLean, G.S. Chandler, J. Chem. Phys. 72 (1980) 5639.
[58] P.B. Armentrout, M.T. Rodgers, J. Oomens, J.D. Steill, J. Phys. Chem. A 112 (2008) 2248.
[59] M.T. Rodgers, P.B. Armentrout, J. Oomens, J.D. Steill, J. Phys. Chem. A 112 (2008) 2258.
[60] A.L. Heaton, P.B. Armentrout, J. Phys. Chem. B 112 (2008) 12056.
[61] A.L. Heaton, V.N. Bowman, J. Oomens, J.D. Steill, P.B. Armentrout, J. Phys. Chem. A 113 (2009) 5519.
[62] P.J. Hay, W.R. Wadt, J. Chem. Phys. 82 (1985) 299.
[63] E.D. Glendening, D. Feller, M.A. Thompson, J. Am. Chem. Soc. 116 (1994) 10657.

[64] J.B. Foresman, A.E. Frisch, Exploring Chemistry with Electronic Structure Methods, Gaussian, Inc., Pittsburgh, PA, 1996.
[65] F. Weigend, R. Ahlrichs, Phys. Chem. Chem. Phys. 7 (2005) 3297.
[66] T. Leininger, A. Nicklass, W. Kuechle, H. Stoll, M. Dolg, A. Bergner, Chem. Phys. Lett. 255 (1996) 274.
[67] D. Feller, J. Comp. Chem. 17 (1996) 1571.
[68] K.L. Schuchardt, B.T. Didier, T. Elsethagen, L. Sun, V. Gurumoorthi, J. Chase, J. Li, T.L. Windus, J. Chem. Inf. Model. 47 (2007) 1045.
[69] S.F. Boys, R. Bernardi, Molec. Phys. 19 (1970) 553.
[70] F.B. van Duijneveldt, J.G.C.M. van Duijneveldt-van de Rijdt, J.H. van Lenthe, Chem. Rev. 94 (1994) 1873.
[71] S. Hoyau, K. Norrman, T.B. McMahon, G. Ohanessian, J. Am. Chem. Soc. 121 (1999) 8864.
[72] D. Feller, E.D. Glendening, M.W. Woon, J. Feyereisen, J. Chem. Phys. 103 (1995) 3526.
[73] D. Feller, Chem. Phys. Lett. 322 (2000) 543.
[74] T.B. McMahon, G. Ohanessian, Chem. Eur. J. 6 (2000) 2931.
[75] D. Feller, E. Apra, J.A. Nichols, D.E. Bernholdt, J. Chem. Phys. 105 (1996) 1940.
[76] B.P. Hay, J.R. Rustad, J.P. Zipperer, D.W. Wester, J. Mol. Struct.: THEOCHEM 337 (1995) 39.
[77] S.M. Smith, A.N. Markevitch, D.A. Romanor, X. Li, R.J. Levis, H.B. Schlegel, J. Phys. Chem. A 108 (2000) 11063.
[78] T.E. Cooper, D.R. Carl, J. Oomens, J.D. Steill, P.B. Armentrout, J. Phys. Chem. A 115 (2011) 5408.
[79] R.G. Wilson, G.R. Brewer, Ion Beams with Applications to Ion Implantation, Wiley, New York, 1973.
[80] C. Lifshitz, Adv. Mass Spectrom. 11 (1989) 713.
[81] S.J. Ye, P.B. Armentrout, J. Phys. Chem. B 112 (2008) 10303.
[82] A.L. Heaton, S.J. Ye, P.B. Armentrout, J. Phys. Chem. A 112 (2008) 3328.
[83] J.D. Steill, J. Oomens, J. Am. Chem. Soc. 131 (2009) 13570.
[84] P.B. Armentrout, S.J. Ye, A. Gabriel, R.M. Moision, J. Phys. Chem. B 114 (2010) 3938.

Table 1. Relative Energies (kJ/mol) at 0 K of 12C4 Conformations Calculated at the B3LYP and MP2(full) Levels of Theory[a]

Symmetry	B3LYP/ 6-311+G(2d,2p)	MP2(full)/ 6-311+G(2d,2p)	B3LYP/ def2-TZVPPD
S_4	0.00	0.00	0.00
D_{2d}	7.3	25.0	4.4
C_s	9.9	18.7	8.6
C_{2v}	36.0	46.0	34.5

Table 2. Fitting Parameters for Eqs. (S1) and (S2), Threshold Dissociation Energies at 0 K, and Entropies of Activation at 1000 K of M^+(12C4) Complexes Produced by ESI[a]

M^+	σ_0 [b]	n [b]	E_0 [c] (eV)	E_0(PSL) [b] (eV)	Kinetic Shift (eV)	$\Delta S^{\ddagger}$(PSL)[b] (J mol^{-1} K^{-1})
Rb^+	11.5 (3.2)	1.4 (0.2)	1.93 (0.05)	1.57 (0.10)	0.36	58 (2)
Cs^+	3.6 (0.9)	1.6 (0.2)	1.66 (0.04)	1.42 (0.09)	0.24	56 (2)

[a] Uncertainties are listed in parentheses. [b]Average values for loose PSL TS. [c]No RRKM lifetime analysis.

Table 3. Fitting Parameters Taken from the Literature and Reanalysis of M^+(12C4) CID Cross Sections: Threshold Dissociation Energies at 0 K and Entropies of Activation at 1000 K[a]

	Previous Analysis					Reanalysis	
M^+	E_0[b] (eV)	E_0(loose) (eV)	$\Delta S^{\dagger}$(loose) (J mol^{-1} K^{-1})	E_0(PSL)[c] (eV)	$\Delta S^{\dagger}$(PSL)[c] (J mol^{-1} K^{-1})	E_0(PSL)[c] (eV)	$\Delta S^{\dagger}$(PSL)[c] (J mol^{-1} K^{-1})
Na^+	4.01 (0.24)	2.37 (0.21)	39 (18)	2.61 (0.13)	64	2.53 (0.13)	67 (2)
K^+	2.40 (0.13)	1.67 (0.16)	41 (18)	1.96 (0.12)	63	1.82 (0.10)	63 (2)
						1.3 (0.1)[d]	63 (2)
						1.96 (0.12)[e]	62 (2)
Rb^+	1.19 (0.04)	0.95 (0.11)	49 (19)	1.06 (0.07)	68	0.95 (0.07)	60 (2)
Cs^+	1.03 (0.08)	0.88 (0.05)	33 (20)	0.96 (0.05)	51	0.87 (0.08)	53 (2)

[a] Analysis of DC-FT data taken from [17] (Na^+), [18] (K^+), and [19] (Rb^+ and Cs^+) and the previous results taken from the same references. Uncertainties are listed in parentheses. [b] No RRKM lifetime analysis. [c] Average values for loose PSL TS obtained using Eq. (S2). [d] Analysis of the tail in the data. [e] Analysis of the data after subtracting the model for the tail.

UU IR Author Manuscript

Table 4. Conversion of 0 K Threshold Energies to 298 K Enthalpies and Free Energies of Dissociation for $M^+(12C4)$

M^+	ΔH_0[a] (kJ/mol)	ΔH_0-ΔH_{298}[b] (kJ/mol)	ΔH_{298} (kJ/mol)	$T\Delta S$[b] (kJ/mol)	ΔG_{298} (kJ/mol)
Na^+	243.9 (12.6)	3.1 (1.7)	247.0 (12.7)	39.5 (4.7)	207.5 (13.6)
K^+	182.0 (17.3)[c]	2.2 (1.4)	184.2 (17.4)	37.9 (5.0)	146.3 (18.1)
Rb^+	151.5 (9.7)	1.5 (1.1)	153.0 (9.8)	36.4 (5.1)	116.6 (11.0)
Cs^+	137.0 (8.7)	1.2 (1.0)	138.2 (8.8)	35.7 (5.1)	102.5 (10.1)

[a] Values from Tables 2 (Rb^+ and Cs^+) and 3 (Na^+ and K^+). [b] Calculated using standard formulae and the rigid rotor/harmonic oscillator approximations. Uncertainties are obtained by varying most frequencies by ±10% along with two-fold variations in the metal-ligand frequencies. [c] Average of the two models listed in Table 3.

Table 5. Bond Dissociation Enthalpies (kJ/mol) of M^+(12C4) Complexes at 0 K

M^+	TCID[a]	MP2[b]			B3LYP[c]		
		D_e	D_0[d]	D_0(cp)[d,e]	D_e	D_0[d]	D_0(cp)[d,e]
Na^+	243.9 (12.6)	280.4	272.8	251.2	264.7	257.2	255.5
		273.1	*265.8*	*248.6*	*267.4*	*260.1*	*255.2*
				255[f]			
K^+	182.0 (17.3)	216.4	210.3	189.3	188.0	181.9	179.0
		208.9	*204.0*	*193.7*	*190.2*	*185.3*	*183.4*
				194[f]			
Rb^+	151.5 (9.7)	207.1	202.4	170.2	160.2	155.4	155.0
		183.6	*179.3*	*156.0*	*150.5*	*146.3*	*144.9*
				163[f]			
Cs^+	137.0 (8.7)	184.2	179.9	159.4	141.7	137.3	137.4
		160.4	*156.8*	*135.0*	*125.6*	*122.1*	*120.4*
				140[f]			
MAD[g]	12.1 (3.9)[h]		38 (11)	14 (8)		4 (6)	5 (5)
			23 (3)	*6 (4)*		*10 (7)*	*9 (6)*
				9 (4)			

[a] Results from Table 4. Uncertainties are listed in parentheses. [b]Calculated at MP2(full)/ def2-TZVPPD and *MP2(full)/HW*/6-311+G(2d,2p)* levels of theory using B3LYP geometries. [c]Calculated at B3LYP/ def2-TZVPPD and *B3LYP/HW*/6-311+G(2d,2p)* levels of theory. [d]Including ZPE corrections with the B3LYP/def2-TZVPPD and *B3LYP/HW*/6-311+G(2d,2p)* frequencies scaled by a factor of 0.98. [e]Also includes counterpoise corrections. [f] MP2/6-31+G(d)//RHF/6-31+G(d) results from Hill et al. [21]. [g] Mean absolute deviation. [h] Average experimental uncertainty.

Figure Captions

Figure 1. Structures and dipole moments of several conformations of 12-crown-4 calculated at the B3LYP/6-311+G(2d,2p) level of theory. Relative energies at 0 K calculated at the B3LYP/def2-TZVPPD (B3LYP/6-311+G(2d,2p), and *MP2(full)/6-311+G(2d,2p)*) levels of theory are also provided.

Figure 2. Side and top views of the cesiated crown are shown along with geometrical parameters of the ground states of the M^+(12C4) complexes for $M^+ = Na^+$, K^+, Rb^+, and Cs^+ (top to bottom) calculated at the B3LYP/def2-TZVPPD level. Bond lengths are in Ångstroms and angles in degrees.

Figure 3. Potential energy surface connecting various conformers of Cs^+(12C4) calculated at the B3LYP/def2-TZVPPD level. Structures for the various intermediates are shown from the top and side. Except for the product asymptote, energies are similar for all other metal cations.

Figure 4. Comparison of dc discharge-flow tube ion source (DC-FT) data from [19] with the present ESI data for collision-induced dissociation of M^+(12C4) where $M^+ = Rb^+$ (part a) and Cs^+ (part b) with Xe as a function of energy in the center-of-mass frame (lower *x*-axis) and the laboratory frame (upper *x*-axis). In both cases, the DC-FT data have been scaled down by a factor of ten.

UU IR Author Manuscript

Figure 5. Cross sections for collision-induced dissociation of Rb^+(12C4) and Cs^+(12C4) produced by ESI (parts a and b) with xenon as a function of kinetic energy in the center-of-mass frame (lower *x*-axis) and the laboratory frame (upper *x*-axis). Solid lines show the best fit to the data using the model of Eq. (S2) convoluted over the neutral and ion kinetic and internal energy distributions. Dotted lines show the model cross sections in the absence of experimental kinetic energy broadening for reactant ions with an internal energy of 0 K. The data and models are shown expanded by a factor of 10 and offset from zero in the insets.

Figure 6. Cross sections for collision-induced dissociation of Na^+(12C4) and K^+(12C4) produced by DC-FT (parts a and b) with xenon as a function of kinetic energy in the center-of-mass frame (lower *x*-axis) and the laboratory frame (upper *x*-axis) taken from [17] and [18]. Solid and dash-dot lines show the best fit to the data using the model of Eq. (S2) convoluted over the neutral and ion kinetic and internal energy distributions. Dotted and dash-dot-dot lines show the model cross sections in the absence of experimental kinetic energy broadening for reactant ions with an internal energy of 0 K. In part b, the dashed line shows the unconvoluted model for the tail. The data and models are shown expanded by a factor of 10 and offset from zero in the insets (dashed line here is convoluted). Solid, dashed, and dotted lines (blue in the online version) show present results, whereas dash-dot and dash-dot-dot lines (red in the online version) show the models of the data using the optimized fitting parameters taken from [17] and [18].

Figure 7. Comparison of the experimental bond energies for M^+-12C4 for M = Na^+, K^+, Rb^+, and Cs^+ with those calculated at the B3LYP(cp) (circles) or MP2(full,cp) (triangles) levels of theory using the def2-TZVPPD basis set. Values taken from Table 5. The full line show perfect agreement between experiment and theory.

UU IR Author Manuscript

Figure 1.

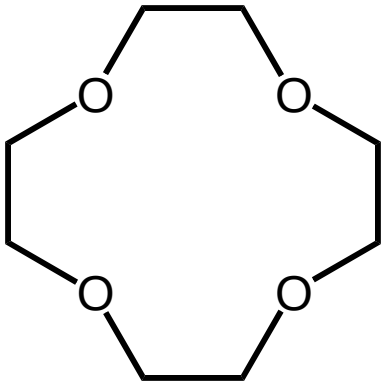

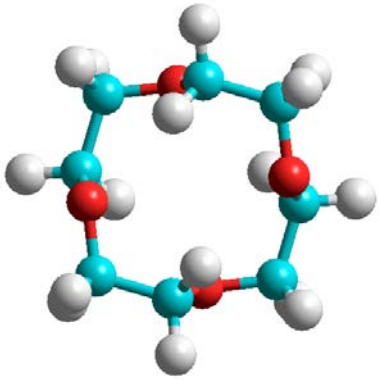

S_4
0.0 (0.0, *0.0*)
kJ/mol
μ = 0.0 D

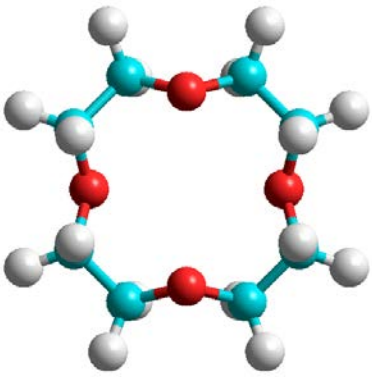

D_{2d}
4.4 (7.3, *25.0*)
kJ/mol
μ = 0.0 D

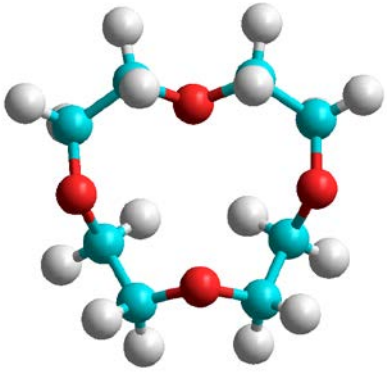

C_s
8.6 (9.9, *18.7*) kJ/mol
μ = 2.82 D

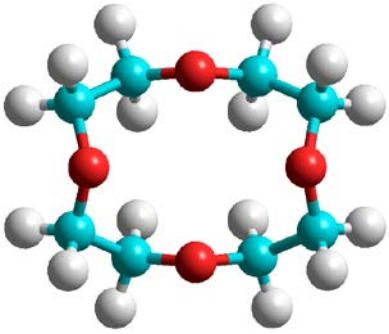

C_{2v}
34.5 (36.0, *46.0*)
kJ/mol
μ = 4.79 D

12-crown-4 (1,4,7,10-tetraoxacyclododecane)

Figure 2.

M^+	R_{MO}	$\angle M\mu_O$
Na^+	2.350	47.1°
K^+	2.749	40.0°
Rb^+	2.933	37.3°
Cs^+	3.098	35.2°

M^+	R_{CO}
Na^+	1.430, 1.433
K^+	1.427, 1.429
Rb^+	1.426, 1.428
Cs^+	1.425, 1.427

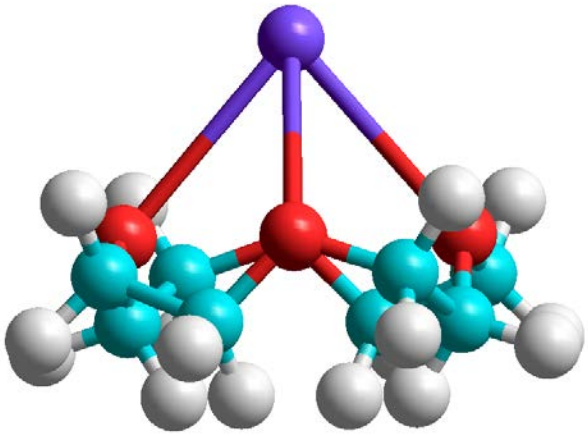

M^+	R_{CC}
Na^+	1.519
K^+	1.519
Rb^+	1.519
Cs^+	1.518

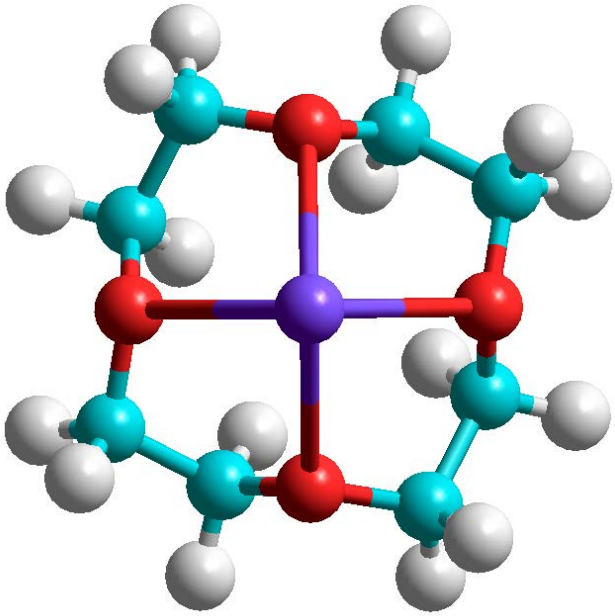

M^+	$\angle OM^+O$
Na^+	73.2°
K^+	62.3°
Rb^+	58.2°
Cs^+	54.9°

M^+	$\angle COCC$
Na^+	83.7°, -164.4°
K^+	81.0°, -163.0°
Rb^+	80.4°, -163.0°
Cs^+	80.0°, -162.8°

M^+	$\angle OCCO$
Na^+	56.3°
K^+	58.4°
Rb^+	58.8°
Cs^+	59.2°

Figure 3.

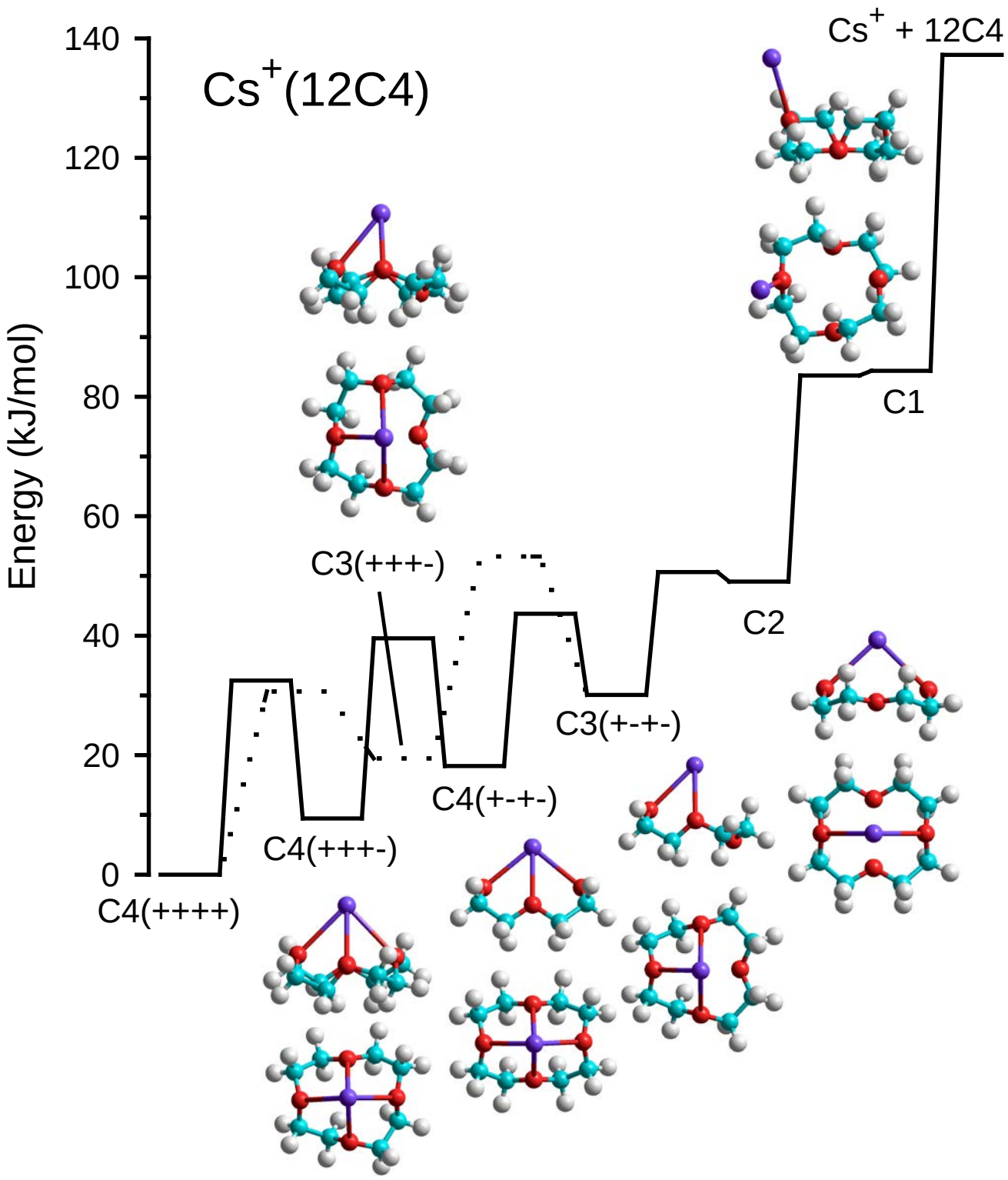
Energy (kJ/mol)
140
120
100
80
60
40
20
0
Cs+(12C4)
Cs+ + 12C4
C1
C2
C3(+++-)
C3(+-+-)
C4(+-+-)
C4(+++-)
C4(++++)

Figure 4.

a.

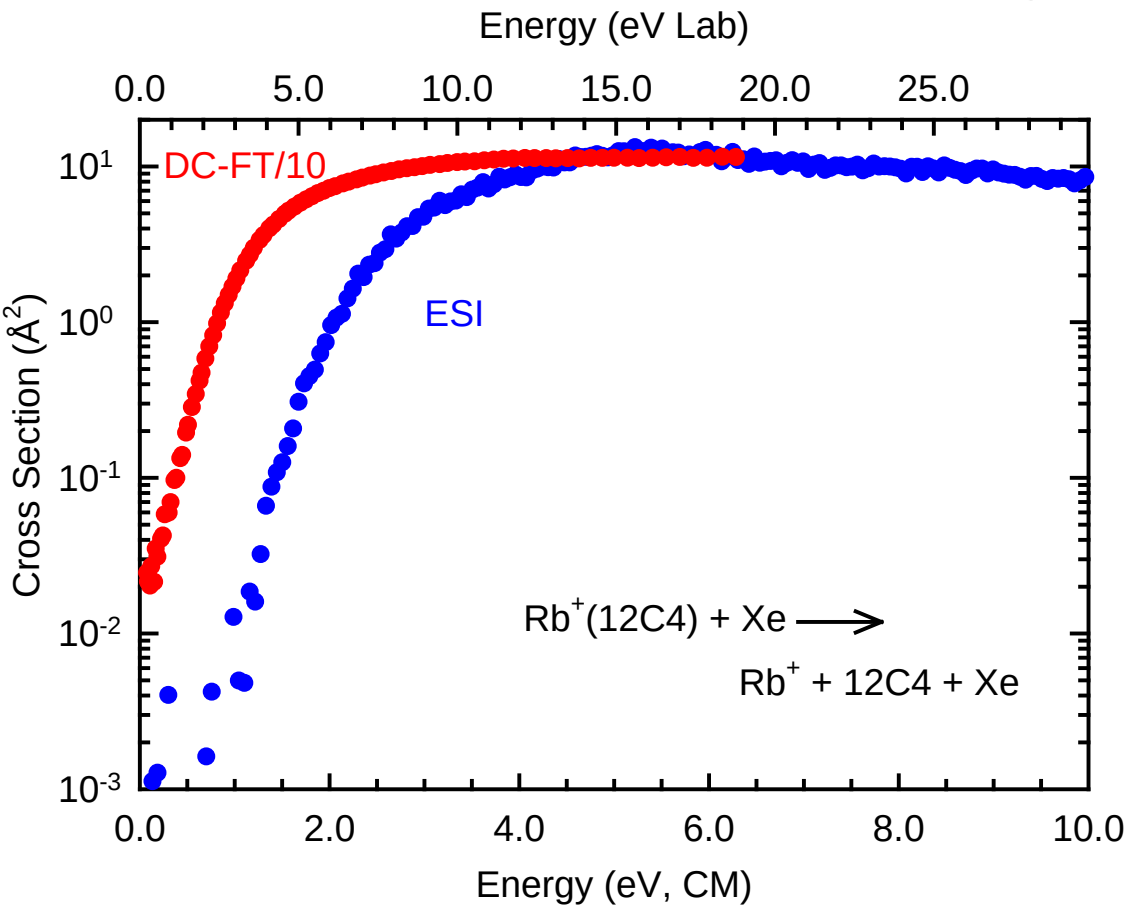
Energy (eV Lab)
0.0
5.0
10.0
15.0
20.0
25.0
DC-FT/10
ESI
Cross Section (Å²)
10¹
10⁰
10⁻¹
10⁻²
10⁻³
Rb⁺(12C4) + Xe
Rb⁺ + 12C4 + Xe
0.0
2.0
4.0
6.0
8.0
10.0
Energy (eV, CM)

b.

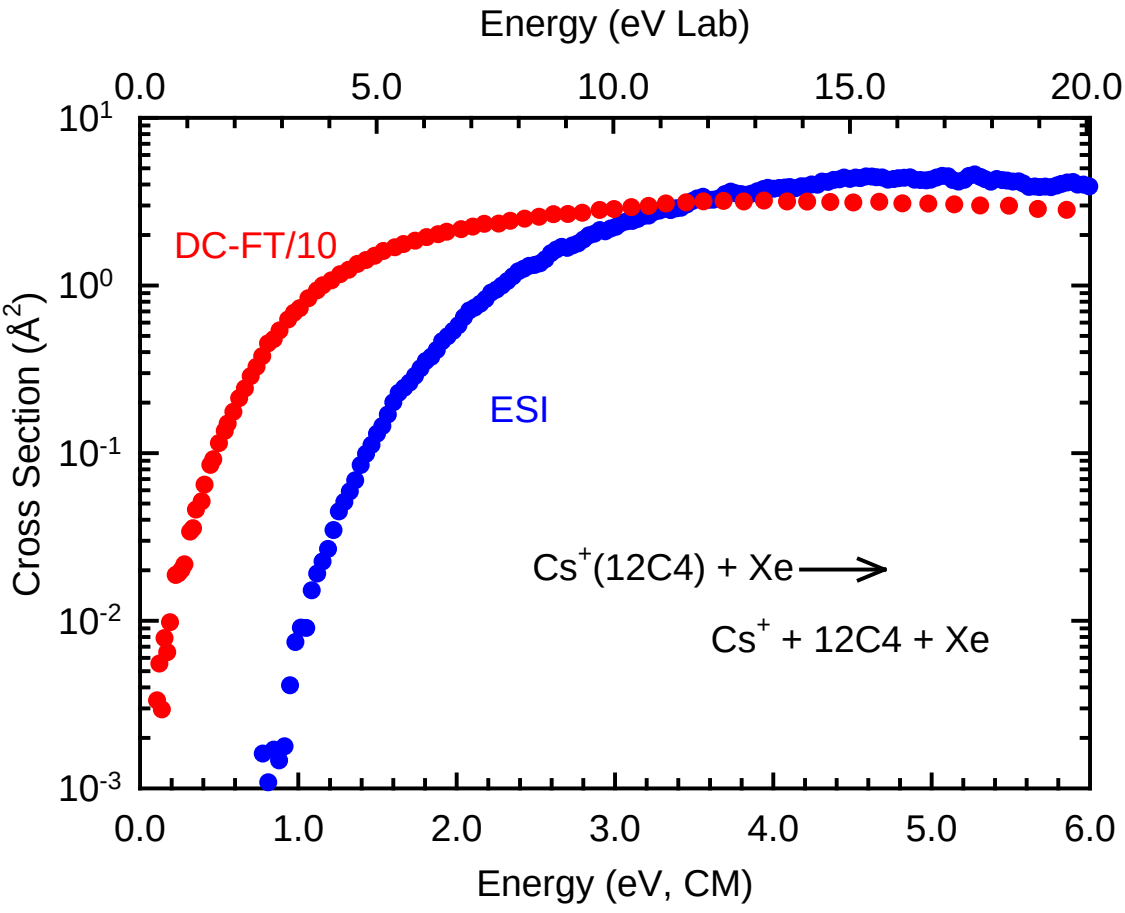
Energy (eV Lab)
0.0
5.0
10.0
15.0
20.0
DC-FT/10
ESI
Cross Section (Å²)
10¹
10⁰
10⁻¹
10⁻²
10⁻³
Cs⁺(12C4) + Xe
Cs⁺ + 12C4 + Xe
0.0
1.0
2.0
3.0
4.0
5.0
6.0
Energy (eV, CM)

Figure 5.

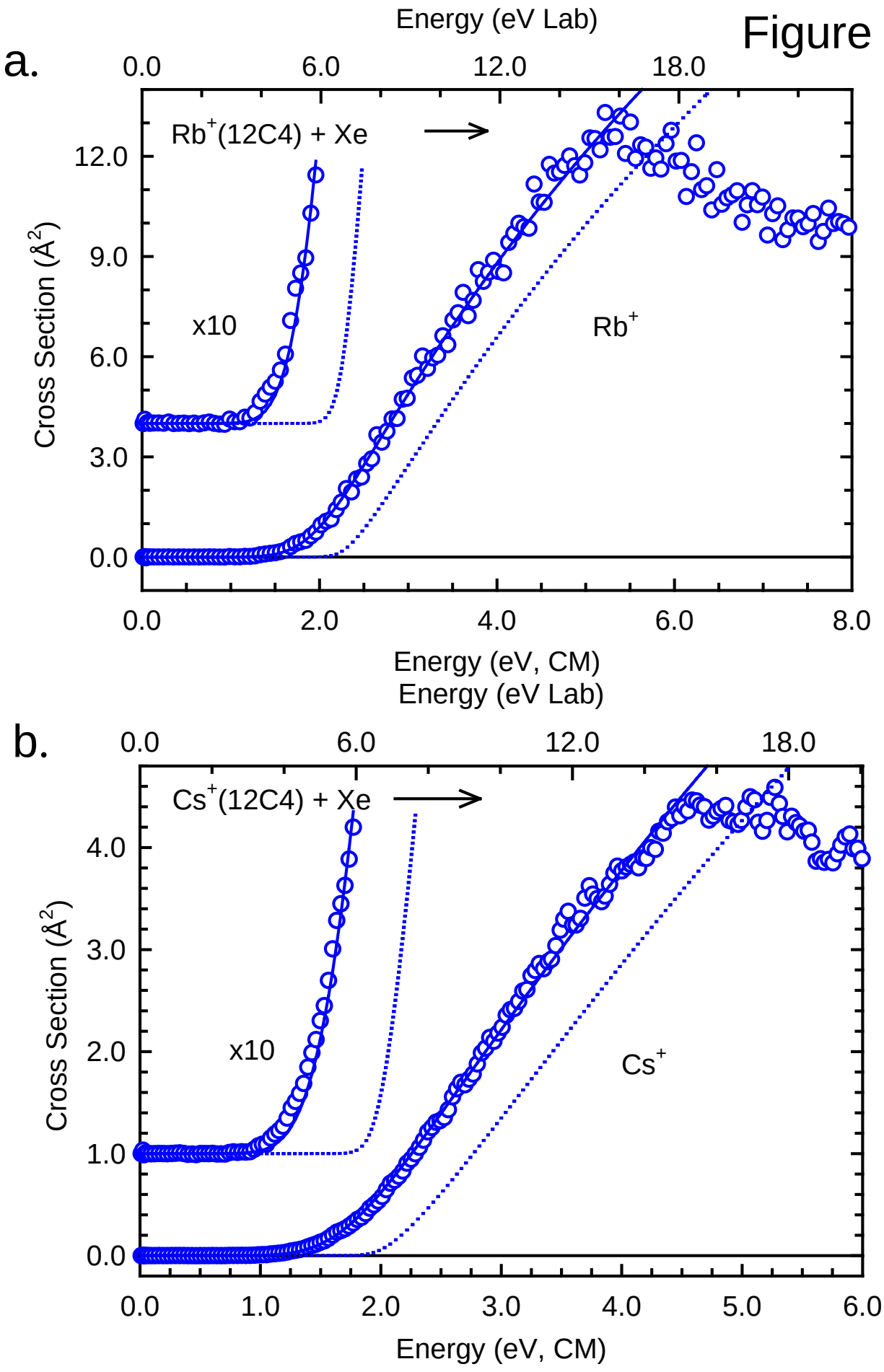
a.
Energy (eV Lab)
0.0
6.0
12.0
18.0
Rb+(12C4) + Xe
x10
Rb+
Cross Section (Å2)
12.0
9.0
6.0
3.0
0.0
0.0
2.0
4.0
6.0
8.0
Energy (eV, CM)
Energy (eV Lab)
b.
0.0
6.0
12.0
18.0
Cs+(12C4) + Xe
x10
Cs+
Cross Section (Å2)
4.0
3.0
2.0
1.0
0.0
0.0
1.0
2.0
3.0
4.0
5.0
6.0
Energy (eV, CM)

Figure 6.

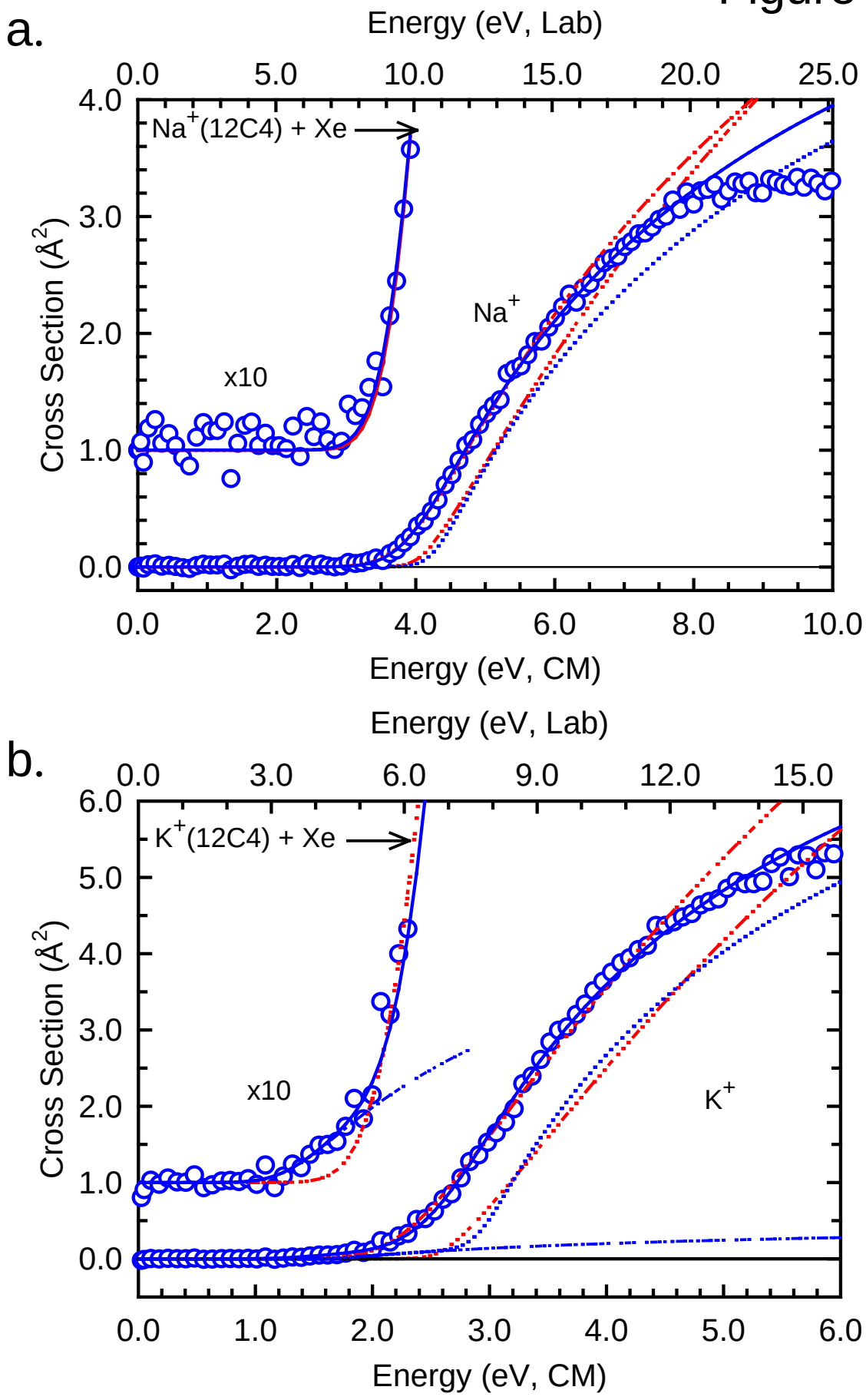
a.
Energy (eV, Lab)
0.0
5.0
10.0
15.0
20.0
25.0
Na+(12C4) + Xe
Cross Section (Å2)
4.0
3.0
2.0
1.0
0.0
x10
Na+
0.0
2.0
4.0
6.0
8.0
10.0
Energy (eV, CM)
b.
Energy (eV, Lab)
0.0
3.0
6.0
9.0
12.0
15.0
K+(12C4) + Xe
Cross Section (Å2)
6.0
5.0
4.0
3.0
2.0
1.0
0.0
x10
K+
0.0
1.0
2.0
3.0
4.0
5.0
6.0
Energy (eV, CM)

Figure 7.

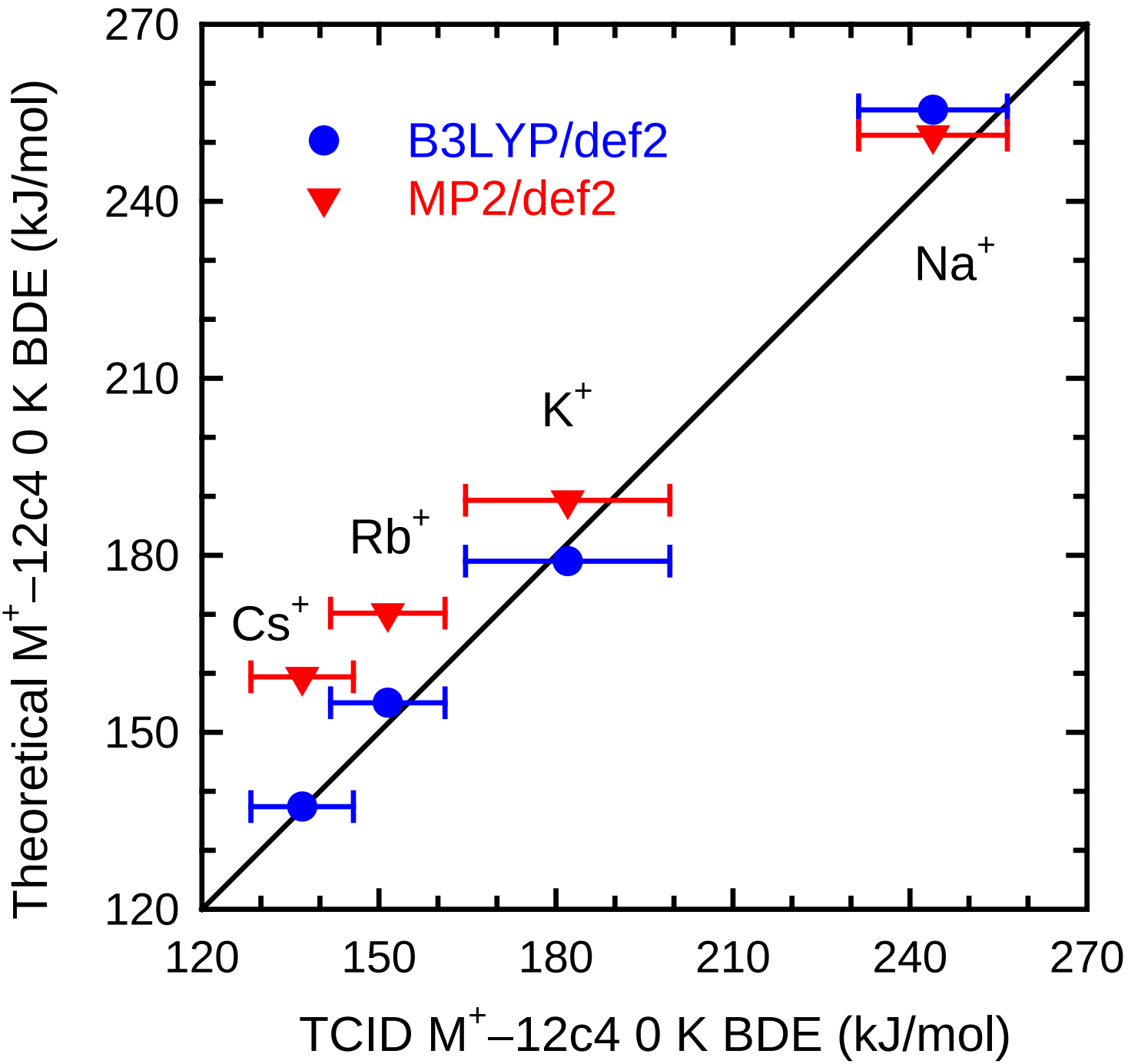
B3LYP/def2
MP2/def2
Na+
K+
Rb+
Cs+
Theoretical M+–12c4 0 K BDE (kJ/mol)
TCID M+–12c4 0 K BDE (kJ/mol)
120
150
180
210
240
270

Supplementary Data for

Alkali Metal Cation Interactions with 12-Crown-4 in the Gas Phase: Revisited

P. B. Armentrout,[a] C. A. Austin,[b] and M. T. Rodgers[b]

[a] *Department of Chemistry, University of Utah, 315 S. 1400 E. Rm 2020, Salt Lake City, UT 84112*

[b] *Department of Chemistry, Wayne State University, Detroit, Michigan 48202*

General Experimental Procedures. Cross sections for CID of the rubidium and cesium cation-12-crown-4 complexes are measured using the Wayne State University guided ion beam tandem mass spectrometer that has been described in detail previously [1]. Experiments are conducted using an electrospray ionization (ESI) source under conditions similar to those described previously [2]. Briefly, the ESI is operated using a 50:50 by volume H_2O/MeOH solution with ~5×10^{-4} M 12C4 and 5×10^{-4} M RbCl or CsCl (all chemicals purchased from Sigma-Aldrich), which is syringe-pumped at a rate of ~1 μL/min into a 35 gauge stainless steel needle biased at ~2000 V. Ionization occurs over the ~5 mm distance from the tip of the needle to the entrance of the capillary, biased at ~35 V. Ions are directed by a capillary heated to 100 °C into a radio frequency (rf) ion funnel [3,4], wherein they are focused into a tight beam. Ions exit the ion funnel and enter an rf hexapole ion guide that traps them radially. Here the ions undergo multiple collisions (>10^4) with the ambient gas and become thermalized. Ions produced in the source are assumed to have their internal energies well described by a Maxwell-Boltzmann distribution of rovibrational states at 300 K, as characterized in previous experiments using a source of similar design [2,5-9].

M^+(12C4) complexes are extracted from the source, focused, accelerated, and mass selected using a magnetic momentum analyzer. The mass-selected ions are decelerated to a well-defined kinetic energy and focused into a rf octopole ion guide that traps the ions radially. The ion guide minimizes losses of the reactant and any product ions resulting from scattering [10]. The octopole passes through a static gas cell containing xenon, which is used as the

UU IR Author Manuscript

collision gas because it is heavy and polarizable, leading to more efficient kinetic to internal energy transfer [11,12]. After collision, the reactant and product ions drift to the end of the octopole where they are extracted and focused into a quadrupole mass filter for mass analysis. The ions are detected with a high voltage dynode, scintillation ion detector [13] and the signal is processed using standard pulse counting techniques. Ion intensities, measured as a function of collision energy, are converted to absolute cross sections as described previously [14]. The uncertainty in relative cross sections is approximately ±5% and that for the absolute cross sections is approximately ±20%. The ion kinetic energy distribution is measured to be Gaussian and has a typical fwhm of 0.2 – 0.5 eV (lab). Uncertainties in the absolute energy scale are approximately ±0.05 eV (lab). Ion kinetic energies in the laboratory frame are converted to energies in the center-of-mass (CM) frame using $E_{CM} = E_{lab}\, m/(m+M)$, where M and m are the masses of the ionic and neutral reactants, respectively. All energies herein are reported in the CM frame unless otherwise noted.

Thermochemical Analysis. Threshold regions of the CID reaction cross sections are modeled using Eq. (S1),

$$\sigma(E) = \sigma_0 \sum_i g_i (E + E_i - E_0)^n / E \qquad \text{(S1)}$$

where σ_0 is an energy-independent scaling factor, n is an adjustable parameter that describes the efficiency of collisional energy transfer [15], E is the relative kinetic energy of the reactants, E_0 is the threshold for dissociation of the ground electronic and rovibrational state of the reactant ion at 0 K. The summation is over the rovibrational states of the reactant ions, i, where E_i is the excitation energy of each state and g_i is the fractional population of those states ($\Sigma g_i = 1$). The Beyer-Swinehart-Stein–Rabinovitch algorithm [16-18] is used to evaluate the number and density of the rovibrational states, and the relative populations g_i are calculated for a Maxwell-Boltzmann distribution at 300 K.

Several effects that obscure the interpretation of the data must be accounted for during data analysis in order to produce accurate thermodynamic information. The first involves energy broadening resulting from the thermal motion of the neutral collision gas and kinetic energy

distribution of the reactant ion. This is accounted for by explicitly convoluting the model over both kinetic energy distributions, as described elsewhere in detail [14]. The second effect considers that Eq. (S1) only models cross sections that represent products formed as the result of a single collision event. To ensure rigorous single-collision conditions, data are collected at three pressures of Xe, generally approximately 0.2, 0.15 and 0.10 mTorr, and the resulting cross sections are evaluated for the pressure effects and extrapolated to zero pressure [19]. The third effect arises from the lifetime for dissociation. As the size of reactant ion complexes increases, so do the number of vibrational modes of the reactant ion and thus the time for energy randomization into the reaction coordinate after collision. Thus, some energized molecules may not dissociate during the time scale of the experiment. This leads to a delayed onset for the CID threshold, a kinetic shift, which becomes more noticeable as the size of the complex increases. These kinetic shifts are estimated by the incorporation of Rice-Ramsperger-Kassel-Marcus (RRKM) statistical theory [20-22], which predicts the unimolecular rate of dissociation of an energized molecule (EM). Application of RRKM theory for analysis of CID thresholds has been described in detail previously [23-26] and transforms Eq. (S1) into Eq. (S2).

$$\sigma(E) = \left(n\sigma_0 / E\right) \sum g_i \int_{E_0 - E_i}^{E} \left(1 - e^{-k(E^*)\tau}\right) \left(E - \varepsilon\right)^{n-1} d\left(\varepsilon\right) \qquad \text{(S2)}$$

Here, ε is the energy transferred from translation into internal energy of the complex during the collision, τ is the time available for dissociation (~ 1.5×10^{-4} s), E^* is the internal energy of the EM after the collision, i.e., $E^* = \varepsilon + E_i$, with n, g_i, E_i, E_0, and E defined above. The term $k(E^*)$ is the unimolecular rate constant for dissociation of the EM as defined in Eq. (S3),

$$k(E^*) = N_{vr}^{+} (E^* - E_0) / h\rho_{vr} (E^*) \qquad \text{(S3)}$$

where h is Planck's constant, $N_{vr}^{\dagger}(E^* - E_0)$ is the sum of rovibrational states of the transition state (TS) at an energy $E^* - E_0$, and ρ_{vr} (E^*) is the density of rovibrational states of the EM at the available energy, E^*. In the limit that $k(E^*)$ is faster than the time-of-flight of the ions, the integration in Eq. (S2) recovers Eq. (S1).

To evaluate the rate constants in Eq. (S3), vibrational frequencies and rotational constants

for the EM and all TSs are required. Because the metal cation-ligand interactions in the complexes studied here are mainly long-range electrostatic interactions (ion-dipole, ion-quadrupole, and ion-induced dipole interactions), the most appropriate model for the TS is generally a loose association of the ion and neutral ligand fragments [27-32], even for multidentate ligands [33-36]. Therefore, the TSs are treated as product-like, such that the TS frequencies are those of the dissociated products. The transitional frequencies are treated as rotors, a treatment that corresponds to a phase space limit (PSL), as described in detail elsewhere [25,37]. The 2-D external rotations are treated adiabatically but with centrifugal effects included [38]. In the present work, the adiabatic 2-D rotational energy is treated using a statistical distribution with an explicit summation over all possible values of the rotational quantum number [25].

The model cross sections of Eqs. (S1) and (S2) are convoluted with the kinetic energy distribution of the reactants and compared to the data. A nonlinear least-squares analysis is used to provide optimized values for σ_0, n and E_0. The uncertainty associated with E_0 is estimated from the range of threshold values determined from different data sets with variations in the parameter n, variations in vibrational frequencies (±10% for all frequencies), changes in dissociation time by factors of 2, and the uncertainty of the absolute energy scale, 0.05 eV (lab).

In deriving the final optimized bond dissociation energies (BDEs) at 0 K, two assumptions are made. First, it is assumed that there is no activation barrier in excess of the endothermicity for the loss of the ligand, which is generally true for ion-molecule reactions and for the heterolytic noncovalent bond dissociations considered here [39]. Second, the measured threshold E_0 values for dissociation are from ground-state reactant ion to ground-state ion and neutral ligand products. Given the relatively long experimental time frame (~1.5×10^{-4} s), incipient products should be able to rearrange to their low-energy conformations after collisional excitation.

UU IR Author Manuscript

Table S1. Relative Energies (kJ/mol) of Stable and Transition State Conformations of M^+(12C4) Complexes Calculated at the B3LYP/def2-TZVPPD Level of Theory[a]

conformer \ M^+ =	Na^+	K^+	Rb^+	Cs^+
C4(++++)	0.0	0.0	0.0	0.0
TSC4(+++(+–))	29.3 (182i)	31.3 (182i)	32.4 (188i)	32.5 (185i)
C4(+++–)	8.0	8.4	9.4	9.4
TSC4(+(+–)+–)	33.5 (180i)	36.8 (183i)	39.0 (175i)	39.5 (178i)
C4(+–+–)	12.4	16.1	17.7	18.2
TSC(4–3)(+++(+–))	29.2 (143i)	30.4 (153i)	31.2 (156i)	30.7 (155i)
C3(+++–)	21.4	21.2	20.8	19.4
TSC3(+(+–)+–)	55.2 (195i)	55.4 (188i)	54.5 (186i)	53.2 (184i)
TSC(4-3)(+–+–)	41.3 (109i)	44.2 (101i)	45.0 (97i)	43.7 (96i)
C3(+–+–)	33.7	32.5 (28i)	31.9	30.2
TSC(3–2)	47.5 (104i)	50.8 (93i)	51.8 (92i)	50.7 (76i)
C2	41.6	46.8	48.6	49.1
TS_{C2-C1}			93.2 (17i)	83.7 (27i)
C1	134.2 (52i)	105.6 (18i)	93.4 (7i)	84.4

[a] Imaginary frequencies (cm^{-1}) in parentheses.

Table S2. Alkali Metal Cation-Oxygen Bond Distances (Å) and $M\mu_O$ Angles (°) of Stable and Transition State Conformations of M^+(12C4) Complexes Calculated at the B3LYP/def2-TZVPPD Level of Theory[a]

conformer \ M^+ =	Na^+	K^+	Rb^+	Cs^+
C4(++++)	2.350(4), 47°(4)	2.749(4), 40°(4)	2.933(4), 37°(4)	3.098(4), 35°(4)
	2.339(4)	*2.757(4)*	*2.988(4)*	*3.218(4)*
TSC4(+++(+–))	2.307, 18°	2.709, 42°	2.890, 39°	3.057, 40°
	2.324, 39°	2.715, 35°	2.908, 34°	3.064, 32°
	2.331, 49°	2.717, 5°	2.920, 1°	3.123, 42°
	2.370, 51°	2.769, 46°	2.953, 44°	3.099, 3°
C4(+++–)	2.318, 45°	2.687, 38°	2.861, 36°	3.020, 33°
	2.332, 50°	2.724, 43°	2.915, 41°	3.083, 39°
	2.352, 49°	2.734, 42°	2.918, 39°	3.087, 36°
	2.383, 37°	2.821, 29°	3.038, 26°	3.250, 25°
TSC4(+(+–)+–)	2.291, 23°	2.682, 40°	2.852, 37°	3.002, 33°
	2.318, 43°	2.683, 37°	2.857, 35°	3.009, 31°
	2.321, 47°	2.715, 14°	2.920, 10°	3.095, 11°
	2.365, 42°	2.809, 34°	3.029, 32°	3.243, 30°
C4(+–+–)	2.304(2), 46°(2)	2.657(2), 38°(2)	2.822(2), 34°(2)	2.966(2), 31°(2)
	2.363(2), 40°(2)	2.821(2), 32°(2)	3.043(2), 30°(2)	3.230(2), 29°(2)
TSC(4-3)(+++(+–))	2.278, 49°	2.657, 40°	2.837, 37°	3.002, 35°
	2.304, 38°	2.747, 44°	2.951, 42°	3.140, 42°
	2.381, 50°	2.771, 44°	2.957, 47°	3.114, 40°
	2.396, 52°	2.801, 46°	2.980, 44°	3.159, 50°

UU IR Author Manuscript

Table S2. Alkali Metal Cation-Oxygen Bond Distances (Å) and $M\mu_O$ Angles (°) of Stable and Transition State Conformations of M^+(12C4) Complexes Calculated at the B3LYP/def2-TZVPPD Level of Theory[a]

conformer	Na	K	Rb	Cs
C3(+++–)	2.257, 51°	2.629, 41°	2.806, 38°	2.960, 35°
	2.345, 49°	2.745, 42°	2.934, 37°	3.104, 35°
	2.374, 52°	2.803, 46°	3.002, 42°	3.191, 38°
	2.439, 74°	2.985, 84°	3.383, 92°	3.642, 95°
TSC3(+(+–)+–)	2.215, 34°	2.624, 36°	2.797, 33°	2.937, 30°
	2.286, 30°	2.731, 38°	2.934, 36°	3.107, 34°
	2.341, 53°	2.732, 6°	2.960, 9°	3.158, 11°
	2.501, 85°	3.700, 115°	3.966, 118°	4.183, 119°
TSC(4-3)(+–+–)	2.222, 42°	2.586, 32°	2.760, 28°	2.910, 24°
	2.235, 28°	2.625, 33°	2.822, 35°	2.984, 38°
	2.464(2), 49°(2)	2.942, 49°	3.147, 49°	3.343, 48°
		2.975, 43°	3.221, 40°	3.442, 40°
C3(+–+–)	2.238, 46°	2.598, 37°	2.764, 34°	2.900, 28°
	2.358(2), 46°(2)	2.796(2), 42°(2)	3.009(2), 37°(2)	3.239(2), 35°(2)
	2.533, 85°	3.239, 100°	3.609, 105°	3.893, 108°
TSC(3-2)	2.176, 22°	2.572, 36°	2.756, 41°	2.901, 44°
	2.364, 83°	2.820(2), 43°(2)	3.029(2), 42°(2)	3.215(2), 40°(2)
	2.382(2), 48°(2)	2.839, 87°	3.079, 89°	3.301, 89°
C2	2.296(2), 48°(2)	2.721(2), 42°(2)	2.913(2), 39°(2)	3.119(2), 39°(2)
	2.324(2), 76°(2)	2.775(2), 81°(2)	2.995(2), 83°(2)	3.146(2), 81°(2)
		2.751(2), 2.757(2)	*2.993(2), 3.046(2)*	*3.247(2), 3.353(2)*

[a] Values in italics from Hill, Feller, and Glendening [40].

References

[1] M.T. Rodgers, J. Phys. Chem. A 105 (2001) 2374.
[2] R.M. Moision, P.B. Armentrout, J. Am. Soc. Mass Spectrom. 18 (2007) 1124.
[3] S.A. Shaffer, D.C. Prior, G.A. Anderson, H.R. Udseth, R.D. Smith, Anal. Chem. 70 (1998) 4111.
[4] S.A. Shaffer, A. Tolmachev, D.C. Prior, G.A. Anderson, H.R. Udseth, R.D. Smith, Anal. Chem. 71 (1999) 2957.
[5] S.J. Ye, P.B. Armentrout, J. Phys. Chem. A 112 (2008) 3587.
[6] A.L. Heaton, R.M. Moision, P.B. Armentrout, J. Phys. Chem. A 112 (2008) 3319.
[7] D.R. Carl, R.M. Moision, P.B. Armentrout, Int. J. Mass Spectrom. 265 (2007) 308.
[8] Y. Chen, M.T. Rodgers, J. Am. Chem. Soc. 134 (2012) 2313.
[9] Y. Chen, M.T. Rodgers, J. Am. Chem. Soc. 134 (2012) 5863.
[10] D. Gerlich, Adv. Chem. Phys. 82 (Part 1) (1992) 1.
[11] N. Aristov, P.B. Armentrout, J. Phys. Chem. 90 (1986) 5135.
[12] N.F. Dalleska, K. Honma, L.S. Sunderlin, P.B. Armentrout, J. Am. Chem. Soc. 116 (1994) 3519.
[13] N.R. Daly, Rev. Sci. Instrum. 31 (1960) 264.
[14] K.M. Ervin, P.B. Armentrout, J. Chem. Phys. 83 (1985) 166.
[15] F. Muntean, P.B. Armentrout, J. Chem. Phys. 115 (2001) 1213.
[16] T.S. Beyer, D.F. Swinehart, Comm. Asso. Computing Machinery 16 (1973) 379.
[17] S.E. Stein, B.S. Rabinovich, J. Chem. Phys. 58 (1973) 2438.
[18] S.E. Stein, B.S. Rabinovich, Chem. Phys. Lett. 49 (1977) 183.
[19] D.A. Hales, L. Lian, P.B. Armentrout, Int. J. Mass Spectrom. Ion Processes 102 (1990) 269.
[20] P.J. Robinson, K.A. Holbrook, Unimolecular Reactions, Wiley Interscience, New York, 1972.
[21] R.G. Gilbert, S.C. Smith, Theory of Unimolecular and Recombination Reactions, Blackwell Scientific, London, 1990.
[22] D.G. Truhlar, B.C. Garrett, S.J. Klippenstein, J. Phys. Chem. 100 (1996) 12771.
[23] S.K. Loh, D.A. Hales, L. Lian, P.B. Armentrout, J. Chem. Phys. 90 (1989) 5466.
[24] F.A. Khan, D.E. Clemmer, R.H. Schultz, P.B. Armentrout, J. Phys. Chem. 97 (1993) 7978.
[25] M.T. Rodgers, K.M. Ervin, P.B. Armentrout, J. Chem. Phys. 106 (1997) 4499.
[26] P.B. Armentrout, K.M. Ervin, M.T. Rodgers, J. Phys. Chem. A 112 (2008) 10071.
[27] R.M. Moision, P.B. Armentrout, J. Phys. Chem. A 106 (2002) 10350.
[28] R.M. Moision, P.B. Armentrout, Phys. Chem. Chem. Phys. 6 (2004) 2588.
[29] F. Meyer, F.A. Khan, P.B. Armentrout, J. Am. Chem. Soc. 117 (1995) 9740.
[30] M.T. Rodgers, P.B. Armentrout, J. Phys. Chem. A 101 (1997) 1238.
[31] H. Koizumi, P.B. Armentrout, J. Am. Soc. Mass Spectrom. 12 (2001) 480.
[32] S.J. Ye, R.M. Moision, P.B. Armentrout, Int. J. Mass Spectrom. 253 (2006) 288.
[33] M.B. More, D. Ray, P.B. Armentrout, J. Phys. Chem. A 101 (1997) 831.
[34] M.B. More, D. Ray, P.B. Armentrout, J. Phys. Chem. A 101 (1997) 4254.
[35] M.B. More, D. Ray, P.B. Armentrout, J. Phys. Chem. A 101 (1997) 7007.
[36] S.J. Ye, P.B. Armentrout, J. Phys. Chem. A 112 (2008) 3587.
[37] M.T. Rodgers, P.B. Armentrout, J. Chem. Phys. 109 (1998) 1787.
[38] E.V. Waage, B.S. Rabinovitch, Chem. Rev. 70 (1970) 377.
[39] P.B. Armentrout, J. Simons, J. Am. Chem. Soc. 114 (1992) 8627.
[40] S.E. Hill, D. Feller, E.D. Glendening, J. Phys. Chem. A 102 (1998) 3813.

UU IR Author Manuscript